Full-field displacement measurement method of metal-as-insulation pancake at liquid nitrogen temperature

Mohamad-Rajab Alharake, Philippe Fazilleau, Aurelien Godfrin, Olivier Hubert

Full-Field Displacement Measurement Method of Metal-as-Insulation Pancake at Liquid Nitrogen Temperature

Mohamad-Rajab ALHarake
DACM
Université Paris-Saclay, CEA
Gif-Sur-Yvette, France
mohamad.alharake@cea.fr

Philippe Fazilleau
DACM
Université Paris-Saclay, CEA
Gif-Sur-Yvette, France
philippe.fazilleau@cea.fr

Aurélien Godfrin
DACM
Université Paris-Saclay, CEA
Gif-Sur-Yvette, France
aurelien.godfrin@cea.fr

Olivier Hubert
LMT
Université Paris-Saclay, ENS Paris-Saclay, CNRS
Gif-Sur-Yvette, France
olivier.hubert@ens-paris-saclay.fr

***Abstract*—In situ measurement of metal-as-insulation (MI) high temperature superconductor (HTS) pancake deformation gives insight to its actual mechanical state. Measurement of hoop strain for inner / outer turn of MI pancake is usually made by strain gauges. This measurement is however local and faces electromagnetic compatibility (EMC) and thermal issues. Non-contact full-field displacement measurement is an interesting alternative solution. This technique is based on digital image correlation (DIC), which derives the displacement field in specified region of interest (ROI) by correlation between the deformed state image and the reference state image.**

In this article, we present a novel DIC experiment setup for displacement measurement of MI pancake in cryogenic cooling. The setup is validated by a cooling test of 304 stainless steel disc. Then, it is used for cooling test of MI pancake made of co-wound copper beryllium - 304 stainless steel tapes. Both tests are done at 80 K by conduction cooling using liquid nitrogen. Finally, experimental results are compared to numerical results obtained from an analytical formulation of the mechanical equilibrium using generalized plane strain assumption.

***Index Terms*—Digital Image Correlation, full-field displacement measurement, Metal-as-Insulation**

I. Introduction

In HTS superconducting magnets, especially at ultra high fields (UHF) [1], magnet sustains high Laplace forces as it increases proportionally to the square of the magnetic field. However, due to slow quench propagation velocity in HTS tapes compared to their LTS counterparts, no-insulation (NI) or metal-as-insulation (MI) HTS magnet configuration is adopted. They are adopted because of their ability to prevent quench by current by-passing at quenched spot with adjacent turns. However, MI provides additional mechanical support when the used metal is stiff. Also, MI dilutes the overall current density, hence the overall volumic magnetic forces as well.

"Nougat" MI HTS insert magnet [2] is an example of UHF MI HTS magnet. It reached 32.5 T, with 14.5 T from HTS insert alone, constituting a world record for this insert size, without being damaged. Using strain gauges to monitor MI HTS pancakes at high fields is limited to local measurements and strain gauge compatibility with the temperature and magnetic field. To circumvent these limitations [3], non-contact full field displacement measurement is done using digital image correlation (DIC) [4] for cooling and powering up of the pancake. DIC has been applied to a large range of situations from room to elevated temperatures [4]. However, DIC application at cryogenic temperature has up to now been limited to [5]–[7] because of cryogenic difficulties (cooling, radiation heat load). Hence, a novel experiment setup has been developed that allows full field displacement measurement of MI HTS pancake in cryogenic cooling (from room temperature to 80 K or lower). In this work, a 304 stainless steel (SS304) disc is tested by cooling to verify the operation of the set-up. Then, a pancake wound with copper beryllium and stainless steel tapes (MI CuBe2 / SS304) that also has SS304 overbanding turns is tested to observe MI pancake displacement by cooling contraction. Experimental results are compared with analytical ones derived from mechanical equilibrium using generalized plane assumption.

II. Experimental Setup

A. Setup Design

Several points are taken into account in the set-up design. The main constraints come from image acquisition and heat load while considering dimensions of the vertical cylindrical cryostat in which the set-up is inserted. This cryostat uses liquid nitrogen and vacuum shielding.

Regarding image acquisition, a clear path between camera, light and the sample is provided using fused silica optical

TABLE I
SAMPLES.

Parameter	Value
SS304 Disc	
Inner / Outer Radius	4 mm / 50 mm
Thickness	4 mm
MI CuBe2 / SS304 Pancake	
Brass 70/30 Mandrel Inner / Outer Radius	22 mm / 25 mm
Brass Width	6 mm
CuBe2 tape Thickness / Width	50 μm / 6 mm
SS304 tape Thickness / Width	50 μm / 6 mm
Number of Turns	50
Number of Overbanding Turns of SS304	7
Pre-Tensioning	$\approx$ 15 N

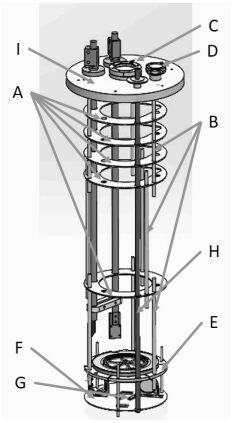

Fig. 1. Setup design: A: aluminum heat shield, B: G10 support rod, C: camera window, D: light window, E: brass support, F: G10 cooling support, G: cooling braid copper clamp, H: cryogenic liquid input tube, I: cryostat flange.

windows on cryostat flange. To maintain clear view of sample during cooling, conduction cooling of sample is considered in the design. Aluminum shields are used as thermal grounding for all sensor wires. Considering image acquisition and cooling in the design (Fig. 1), a setup was manufactured.

B. DIC Setup

A LabVIEW program is used to monitor and synchronize the image acquisition with the temperature measurements of the sample, the brass support, and others parts of the setup. The camera is triggered with a trigger cable that is connected to a relay controlled by NI 9269 module using LabVIEW. Images are saved directly on the computer using EOS utility program, which also allows live view of the sample.

Images are captured using Canon camera EOS 5D Mark IV with Canon lens EF 70 - 200 mm f/4L IS USM being used at 200 mm focal length. The sample is illuminated by a constant white light from a LED pointer (Effilux-Sharp-FL-FF, 5W). With camera being at stand-off distance approximately 1300 mm from sample, the camera is adjusted to have good quality images using ISO 800, aperture F8.0, shutter speed 1 / 400 s, and raw image quality (6720 x 4480 pixels). The camera set-up is mounted outside the cryostat at room temperature and adjusted. Then, images are analyzed with Correli 3.0 code [8] that is developed by LMT ENS Paris Saclay.

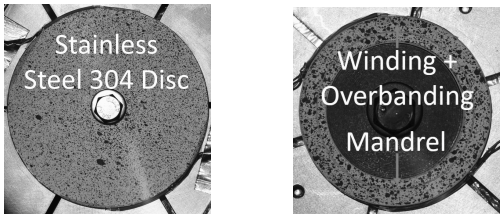

(a) (b)

Fig. 2. (a) SS304 Disc; (b) MI CuBe2 / SS304 pancake.

C. Experimental Procedure

Speckle pattern is applied on sample by spraying Boron Nitride white layer on it then a fine spray of black matt paint to get randomized small black dots. Boron nitride speckle layer is chemically inert and electrically insulating [9]. Thus, it is suitable to be used with superconducting magnets for cooling or energizing processes. The black speckle is placed upon the boron nitride layer to benefit from the latter's properties. A relevant pattern should lead to a wide contrast between black and white while being non-repetitive and isotropic to enhance greyscale detection for DIC measurement. The sample is centered on brass support disc using a centering screw. Then, pancake and set-up are inserted inside the cryostat (leak tight). To avoid ice formation inside the cryostat, a nitrogen atmosphere is created inside of it by flushing with nitrogen gas three times. Finally, the LabVIEW program, which acquires temperature measurement and synchronizes image capturing, is started when the cryostat is filled with liquid nitrogen till it reaches the level below the brass support. For sample conduction cooling, tinned copper braids are immersed in the liquid bath and clamped onto brass support cooling sample by contact. Adjusting manually the liquid nitrogen flow, we can control the cooling speed of the test. The cooling speed was approximately $2.1°C/min$. Images are acquired from room to cryogenic temperature (80 K) (1 image every 30 s), and the temperature acquisition rate is 10 Hz.

III. Cooling Tests and Result Analysis

A. DIC Results

SS304 disc (Table I for dimensions, Fig. 2a) is cooled down from 296 K to 80 K. Displacement measurement during thermal contraction from 296 K to 80 K is done using DIC. DIC compares images at deformed state (80 K) to that of reference state (296 K) in the ROI defined by the mesh of element size (Elsize) 71 pixels (Fig. 3e) (scale: 1 pixel: $\frac{1}{31}$ mm) to get the field displacement. DIC [10] is based on the principle of gray-level conservation; i.e. it is conserved between referenced image f(x) and deformed image g(x). Its only variation is due to displacement $u(x)$:

$$f(x) = g(x + u(x)) \tag{1}$$

The sought displacement field minimizes the sum of squared differences in the ROI:

$$\Phi_c^2 = \int_{ROI} (f(x) - g(x + u(x)))^2 dx \tag{2}$$

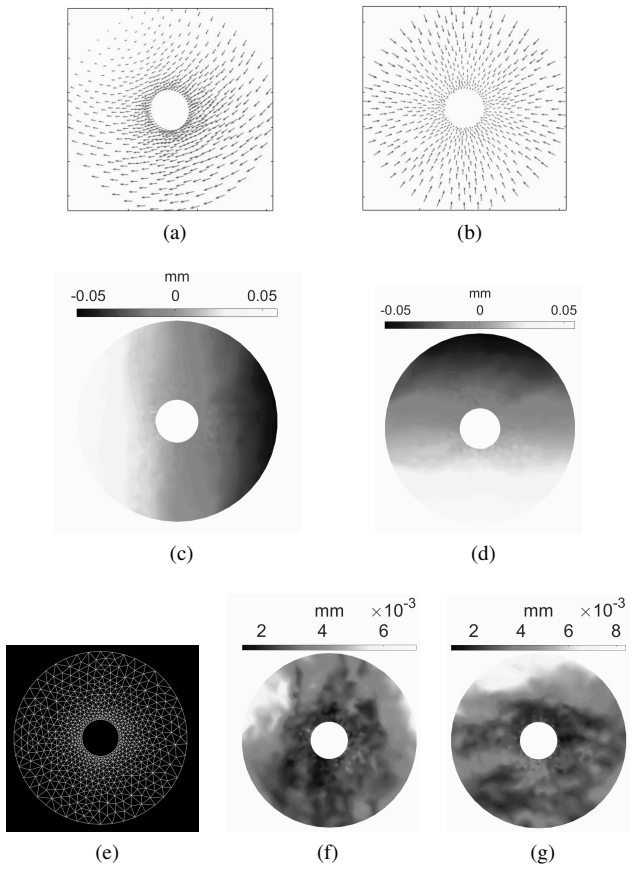

Fig. 3. SS304 disc: (a): Displacement Vectoring of DIC result without rigid body motion elimination (RBME); (b): Displacement Vectoring of DIC result with RBME; (c) / (d): Ux / Uy Field Displacement of DIC with RBME; (e): TRI3 mesh of Elsize 71 pixel of SS304 disc; (f) / (g): Standard deviation of DIC Ux / Uy displacement.

The minimization of Φ_c^2 is non-linear; thus, weak formulation is chosen where displacement field is discretized as:

$$u(x) = \Sigma_n a_n \psi_n(x) \tag{3}$$

ψ_n is an n-th polynomial spatial function, and a_n corresponds to the associated degrees of freedom. This global approach of DIC (ROI) [10] gives rise to the TRI3 mesh used in the DIC calculation in this article.

It is noticed from Fig. 3a that results are not in accordance with thermal contraction phenomenon (contraction towards center). This discrepancy is due to presence of rigid body motion (RBM) [11] (translation and / or rotation). RBM is the pure translation or rotation of the sample that does not result from any deformation of the sample. This movement is measured along with the actual displacement by DIC resulting in an incomplete DIC result that requires post-processing.

Hence, to get the DIC displacement, rigid body motion should be removed from measured displacement, which can be written as follows:

$$u^{'} = u + u^{RBM} \tag{4}$$

where $u^{'}$, u and u^{RBM} are, respectively, the measured displacement, the DIC displacement, and the rigid body motion displacement. Rotation and translation of RBM are considered small in the experiment, expressed as follows:

$$u^{RBM} = (t_x e_x + t_y e_y + \theta(-y_i e_x + x_i e_y)) \tag{5}$$

where x_i, y_i are the mesh node coordinates, t_x, t_y are the translations in x and y directions, and θ is in plane rotation angle. Finding parameters of u^{RBM} is done using linear least squares fit:

$$min\Sigma_i ||u(x_i) - (t_x e_x + t_y e_y + \theta(-y_i e_x + x_i e_y))||^2 \tag{6}$$

After removing RBM, DIC displacement corresponds to thermal contraction as illustrated in Figs. 3b, 3c, and 3d. Results are in accordance with the thermal contraction direction (towards the center). Also, Figs. 3f and 3g show negligible variation in DIC measurement of Ux and Uy at the same temperature. The variation is calculated as standard deviation of DIC measurement over several images (17 images) at the same cryogenic temperature (80 K).

B. Comparison with Analytic Calculation

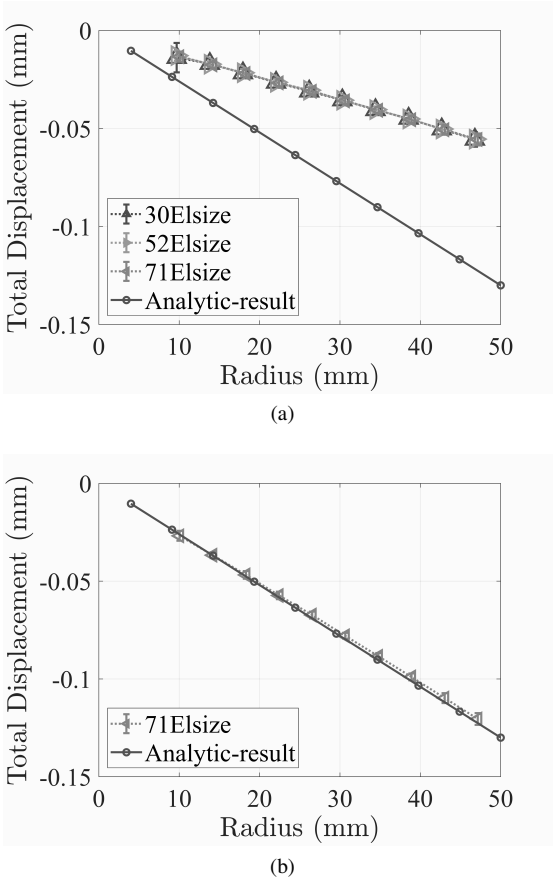

Fig. 4. Cooling test of SS304 Disc: (a): DIC displacement using different meshes and analytic displacement; (b): Actual displacement (DIC displacement after adding setup contraction effect, $\alpha_T = -13.86$ E-4 mm/mm, 71 pixels Elsize chosen because the higher mesh size the lower DIC noise).

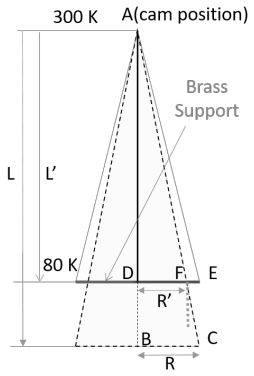

Fig. 5. Setup contraction sketch: position of brass support is dotted at reference (room temperature) state and solid at low temperature (at 80 K).

A representative radial displacement is calculated from averaging over several radial measurements for different angles from 0 to 2 π.

$$u_T(r_k) = \frac{1}{n}\sum_{1}^{n} u_{FT}(r_k)(\theta_i) \tag{7}$$

where u_T and u_{FT} are respectively the mean total radial displacement at a given radius and the total radial displacement at a mesh point from field displacement.

The experimental displacement is compared to the displacement of an analytic calculation using generalized plane strain assumption (see the Appendix) with Fig. 4a showing significant difference between the two results whatever the mesh size (error bar being standard deviation of u_{FT}). We explain this difference as the result of an axial setup contraction that moves the sample closer to camera. The deformed image is taken after setup contraction, the sample being slightly closer to camera than its initial position, and thus enlarging it slightly. Hence, DIC displacement is the sum of actual displacement of sample and magnification (apparent) displacement due to setup axial contraction. With sample being circular and the magnification being uniform, magnification effect is a constant positive radial strain (Fig. 5).

We denote as α_T the total set-up contraction. The latter is calculated using the temperature measurements via a series of thermocouples and the thermal contraction of G10 support rods. It is expressed as follows:

$$\alpha_T = \int_{T1}^{T2} \alpha(T)dT \tag{8}$$

where T1 greater than T2 and $\alpha(T)$ is thermal contraction coefficient of G10 rod [12]. It yields to a total contraction α_T = -13.86$\times 10^{-4}$ mm/mm. In addition, α_T can be expressed in another way as "$\alpha_T = \frac{L'-L}{L}$", where L and L' are distances from flange to brass support before and after setup contraction respectively.

Sample remains in the field of view of camera even after contraction. Fig. 5 shows that a part is apparently outside of reference field of view. This part represents the magnification

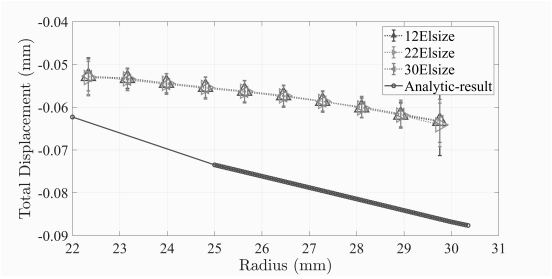

(a)

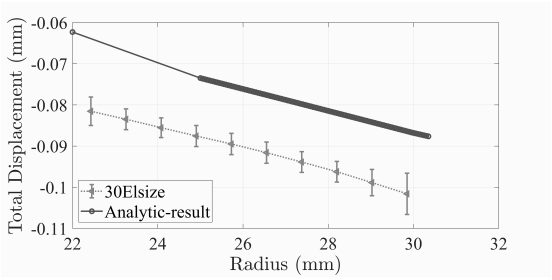

(b)

Fig. 6. Cooling of MI CuBe2 / SS304 pancake: (a): DIC displacement using different meshes and analytic displacement (290 K to 80 K) (12 / 22 / 30 pixels Elsize were chosen because a smaller speckle area requires a smaller mesh size)); (b): DIC displacement after adding setup contraction effect) ($\alpha_T = -12.9\times 10^{-4}$ mm/mm, 30 Elsize chosen because higher the mesh size, lower the DIC noise).

effect of setup contraction, and it can be expressed as apparent strain ($\frac{R'}{R} = \frac{L'}{L}$ from Fig. 5):

$$\epsilon_{rr} = \frac{R-R'}{R} = \frac{L-L'}{L} = -\alpha_T \tag{9}$$

Hence, actual contraction displacement of SS304 disc is expressed as follows:

$$u_r = u_{rDIC} - u_{rimage} = u_{rDIC} - r\epsilon_{rr} \tag{10}$$

where r, u_{rDIC} and u_{rimage} are respectively a radial position, the DIC displacement without RBM and the displacement caused by image magnification due to setup contraction.

Fig. 4b shows that the difference between analytic and actual displacement is small. It is only due to total contraction calculated using temperature measurement from sensors placed on current leads and not G10 rods. Since experimental The cooling test of SS304 disc showed that the conduction cooling used achieved good result (80 K), the image acquisition procedure yielded good images for proper DIC calculations, the speckle functioned without cracking or peeling, and the DIC measured displacement is in accordance with the analytical one. Thus, the use of DIC at cryogenic conditions is applicable, and the set-up is functional for DIC measurements.

After this simplified test, MI CuBe2 / SS304 pancake (Fig. 2b) has been tested. It is cooled down from 290 K to 80 K. Mechanical regularization [13] is used in DIC calculation of MI pancake to minimize noises. It is used because speckle area is small and few pixels cover it. The width of speckle

area is ≈ 240 pixels, while image size were of 6720×4480 pixels. Regularization length used in DIC is 24 pixels.

Total displacement amplitude of MI pancake is lower than that predicted by the analytic calculation without considering setup contraction (Fig. 6a) with negligible mesh size sensitivity (Fig. 6a). When the set-up contraction correction (α_T = -12.9×10^{-4} mm/mm, this value differs from the previous one since temperatures measured along the rod are slightly different from temperatures observed during SS304 cooling) is applied (Fig. 6b), experimental amplitudes become higher than analytic ones by approximately 0.02 mm. This discrepancy could be explained by a wrong evaluation of temperature due to a bad positioning of temperature sensors, or the fact that G10 support rods are insulating materials that have low thermal conductivity. This might cause the temperature distribution along the G10 to be different than the temperature measured. Additional tests are needed to specify the cause of this discrepancy.

IV. Conclusion

A novel setup has been designed that allows full field displacement measurement of MI pancakes at cryogenic temperatures. Rigid body motion elimination and setup contraction effect had to be implemented to acquire the actual displacement. Moreover, proper speckle preparation and DIC setup calibration are important to get relevant results [4] as image and speckle quality affect DIC results. In addition, a precise temperature measurement of G10 support rods is necessary for proper calculation of setup contraction effect.

A liquid nitrogen cooling test, of a SS304 disc allowed for the validation of the set-up. It showed that the speckle used does work at cryogenic temperature, and that DIC yields proper results. In addition, as shown from MI CuBe2 / SS304 test, more tests are required to pinpoint the reason for the discrepancy observed between analytic and experimental results carried out with a MI CuBe/SS304 co-wound pancake. A next step will consist in cooling all set-up at liquid helium temperature making the MI HTS REBCO pancake superconducting and observe the displacement fields due to Laplace forces during an energizing test.

Appendix
Generalized Plane Strain cooling

$$u'' + \frac{u'}{r} - k^2\frac{u}{r} = -\frac{C_{rz}-C_{\theta z}}{C_{rr}}\epsilon_z^{tot} + \frac{C_{rr}-C_{\theta r}}{C_{rr}}\alpha_r + \frac{C_{\theta r}-C_{\theta\theta}}{C_{rr}}\alpha_\theta + \frac{C_{rz}-C_{\theta z}}{C_{rr}}\alpha_z \quad (11)$$

where u, r, C_{ij}, k, α_r, α_θ, and α_z are respectively the radial displacement, the radius, the orthotropic stiffness coefficients, k an anisotropy factor ($k^2 = \frac{C_{\theta\theta}}{C_{rr}}$), the radial, hoop, and axial thermal contraction. ($'$) and ($''$) denote the first and second order radial derivatives.

References

[1] R. Gupta et al., "Status of the 25 T 100 mm bore HTS solenoid for an axion dark matter search experiment", IEEE Trans. Appl. Supercond., vol. 29, no. 5, Aug. 2019.

[2] Philippe Fazilleau, Xavier Chaud, François Debray, Thibault Lecrevisse, and Jung-Bin Song "38 mm diameter cold bore metal-as-insulation HTS insert reached 32.5 T in a background magnetic field generated by resistive magnet". In: Cryogenics 106 (Mar. 2020)

[3] Y. Kim, et al., "Strain in YBCO double-pancake coil with stainless steel overband under external magnetic field" IEEE Trans. Appl. Supercond., vol. 25, no. 3, Jun. 2014, Art. ID 4300504.

[4] International Digital Image Correlation Society, Jones, E.M.C. and Iadicola, M.A. (Eds.) (2018). A Good Practices Guide for Digital Image Correlation.

[5] H C Zhang, C J Huang, and L F Li "Liquid helium free cryogenic mechanical property test system with optical windows", 2017 IOP Conf. Ser.: Mater. Sci. Eng. 278 012083

[6] Wang X, Zhou Y, Guan M, Xin C. "A versatile facility for investigating field-dependent and mechanical properties of superconducting wires and tapes under cryogenic-electro-magnetic multifields". Rev Sci Instrum. 2018 Aug;89(8):085117.

[7] J. Pelegrin and W. O. S. Bailey and D. A. Crump "Application of DIC to extract full field thermo-mechanical data from an HTS coil" . IEEE Trans. Appl. Supercond., vol. 28, no. 4, Jun. 2018

[8] Leclerc H, Neggers J, Mathieu F, Hild F and Roux S 2015 Correli 3.0, IDDN. FR. 001.520008. 000. SP 2015.000.31500 Agence pour la Protection des Programmes Paris (France)

[9] "Boron Nitride Application". Accessed: July 22,2021.[Online]. Available:https://www.bn.saint-gobain.com/

[10] F. Hild, S. Roux. "Comparison of local and global approaches to digital image correlation". Exp. Mech., 52 (2012), pp. 1503-1519.

[11] A.S. Chernyatin, Yu.G. Matvienko, and P. Lopez-Crespo. "Mathematical and numerical correction of the DIC displacements for determination of stress field along crack front". In: Procedia Structural Integrity 2 (2016), pp. 2650-2658.

[12] "NIST, Index of Material Properties, Properties of solid materials from croygenic to room temperatures". Accessed: June 28,2021.[Online]. Available: https://trc.nist.gov/cryogenics/materials/materialproperties.htm

[13] Zvonimir Tomicevc, Francois Hild, and Stephane Roux. "Mechanics-aided digital image correlation". In: The Journal of Strain Analysis for Engineering Design 48.5 (June 2013), pp. 330-343.

[14] J. W. Ekin, "Experimental Techniques for Low Temperature Measurements", Oxford University Press, (2006)